Lattice Boltzmann Numerical Prediction of Flow Behavior Downstream of Cylinder Blockage at Various Reynolds Numbers

Che Sidik N. Azwadi, and Samion Syahrullail

***Abstract*—**This paper presents numerical results of flow behavior downstream of cylinder blockage at various Reynolds numbers. The lattice Boltzmann method, a numerical scheme based on mesoscopic approach has been used as a computational tool to study the vortices formation downstream of the cylinder. In this study, three different types of blockage are located inside a channel and the effect of the shape of blockage on the flow behavior downstream of cylinder at various Reynolds number is investigated extensively. Comparisons of detailed flow pattern for every case via streamline and length of vortices have been carried out. The ability of the lattice Boltzmann numerical scheme to simulate complicated flow phenomena is demonstrated.

***Keywords*—**CFD, lattice Boltzmann, cylindrical blockage, channel flow.

I. Introduction

LATTICE Boltzmann (LB) model, a model based on the physical at the mesoscopic scale, has received much attention since the 1980s due to its simplicity and easy implementation. Due to their ability to incorporate particle interactions at the mesoscopic level, LB models fit for simulating the behavior of complex flow system [1]. It has also been proven to be a useful tool for solving a wide range of complex flows, such as turbulent [2], flow inside porous media [3], immiscible fluid [4], magnetohydrodynamics [5], and many others [6][7][8].

In this paper, a BGK lattice Boltzmann model [9] will be considered for single isothermal fluid flow system. Two-dimensional channel flow with three types of blockage at various Reynolds numbers are solved. Comparisons in terms of vortex behavior downstream the blockage are presented. The objective of this paper is to demonstrate the capability of lattice Boltzmann BGK method and to stimulate further studies using the lattice Boltzmann approach.

Section *II* presents a basic theory of the lattice Boltzmann model used in this paper that will enhance the general reader's understanding of this simulation method. The lattice Boltzmann simulation of channel flow with blockage is discussed in Section *III*. Results obtained by others simulation method are also brought for comparison purposes. The final section contains concluding remarks.

C. S. Azwadi is with the Faculty of Mechanical Engineering, Universiti Teknologi Malaysia, Skudai, 81310 UTM Skudai, Johor, Malaysia (corresponding author to provide phone: 607-553-4718; fax: 607-556-6159; e-mail: azwadi@fkm.utm.my).

S. Syahrullail is with the Faculty of Mechanical Engineering, Universiti Teknologi Malaysia, Skudai, 81310 UTM Skudai, Johor, Malaysia (corresponding author to provide phone: 607-553-4661; fax: 607-556-6159; e-mail: syahruls@fkm.utm.my).

II. Lattice Boltzmann Method

A. Lattice Boltzmann Equation

The governing lattice Boltzmann equation (LBE), discretized in time and space, is given by

$$f(\mathbf{x}+\mathbf{c}\Delta t, t+\Delta t) - f(\mathbf{x},t) = \Omega(f) \tag{1}$$

where f is the particle distribution function with constant velocity $\mathbf{c}$ at position $\mathbf{x}$ and time t and $\Omega(f)$ is collision integral. One of the major problems when dealing with LBE is the complicated nature this collision integral. Any replacement of collision must satisfy the conservation of mass, momentum and energy. The idea behind this replacement is that the large amount of detail of two-body interaction is not likely to influence significantly the values of many experimental measured quantities [10]. There are few versions of collision functions published in literature. However, the most well accepted version due to its simplicity and efficiency is the Bhatnagar-Gross-Krook (BGK) model [9]. The equation that represents this model is given by

$$\Omega(f) = -\frac{1}{\tau}\left(f - f^{eq}\right) \tag{2}$$

where f^{eq} is the equilibrium distribution function. τ is the time to reach equilibrium condition during collision process and often called as time relaxation. Equation (2) of the BGK collision model describes that $1/\tau$ of non-equilibrium distribution function relaxes to equilibrium state within time τ on every collision process. Substitute (2) in (1) gives

$$f(\mathbf{x}+\mathbf{c}\Delta t, t+\Delta t) - f(\mathbf{x},t) = -\frac{1}{\tau}\left(f - f^{eq}\right) \tag{3}$$

Equation (3) consists of two parts; propagation (left hand side) which refers to the propagation of the distribution function to the next node in the direction of its velocity and collision (right hand side) which represents the collision of the particle distribution function. In LBM, magnitude of $\mathbf{c}$ is set up so that in each time step Δt, every distribution function propagates in a distance of lattice node spacing Δx. This will

ensure that the distribution function arrives exactly at the lattice node after Δt and collide simultaneously.

The number of assigned microvelocity to the distribution function will determine its lattice model. The general form of the lattice velocity model is expressed as DnQm where D represents spatial dimension and Q is the number of connection (lattice velocity) at every node [11]. For two-dimensional simulation, there are D2Q7, D2Q9, D2Q17, D2Q52, etc lattice models have been tried by researchers. The choice of lattice model is depend on the order of tensor needed to recover macroscopic equations. For example, D2Q52 is required to correctly recover energy equation with correct energy flux term [12].

In present study, the D2Q9 has been chosen due to its flexibility and efficient for boundary treatment [13]. The microscopic velocity components for this model are

$$\mathbf{c} = \begin{bmatrix} 0 & 1 & 0 & -1 & 0 & 1 & -1 & -1 & 1 \\ 0 & 0 & 1 & 0 & -1 & 1 & 1 & -1 & -1 \end{bmatrix} \tag{4}$$

The lattice geometry is shown in Fig. 1.

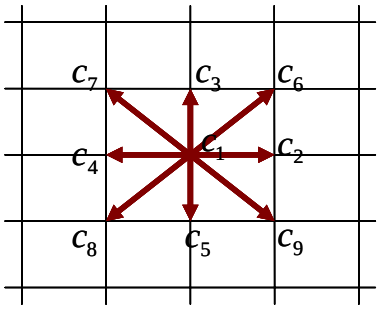

Fig. 1 D2Q9 lattice geometry

The equilibrium distribution function of the D2Q9 model is

$$f_{i\alpha}^{eq} = \rho w_\alpha \left[1 + 3(\mathbf{c}_{i\alpha} \cdot \mathbf{u}) + \frac{9}{2}(\mathbf{c}_{i\alpha} \cdot \mathbf{u})^2 - \frac{3}{2}\mathbf{u}^2 \right] \tag{5}$$

where the value of weights are depend on the types of velocity direction

$$w_0 = \frac{4}{9},\ w_1 = \frac{1}{9} \text{ and } w_2 = \frac{1}{36} \tag{6}$$

Noted also the subscript i, ($i = 1,2,..,9$) have been used in (5) to describe the number of microscopic velocity directions. Here $\alpha = 0$ when $i = 0$, $\alpha = 1$ when $i = 2,3,4,5$ and $\alpha = 2$ when $i = 6,7,8,9$. Therefore, (3) can be rewritten in discretized form in terms of microscopic velocity as follow

$$f_{i\alpha}(\mathbf{x} + \mathbf{c}_{i\alpha}\Delta t, t + \Delta t) - f_{i\alpha}(\mathbf{x}, t) = -\frac{1}{\tau}\left(f_{i\alpha} - f_{i\alpha}^{eq}\right) \tag{7}$$

D2Q9 has been proved to satisfy up to fourth order tensor [14]. Under this constraint, the macroscopic variables such as density and velocity can be obtained by moment integration of distribution function as follow

$$\sum_{\alpha=0}^{2}\sum_{i=1}^{9} f_{i\alpha} = \rho,\ \sum_{\alpha=0}^{2}\sum_{i=1}^{9} \mathbf{c}_{i\alpha} f_{i\alpha} = \rho\mathbf{u} \tag{8}$$

B. Derivation of Macroscopic Equations

In this subsection, the derivation of continuity and Navier-Stokes equations by using the so-called *Chapmann-Enskog* expansion is discussed. To see this, the Taylor series expansion is applied of left hand side of (7) and retaining terms up to second order gives

$$(\partial_t + \nabla \cdot \mathbf{c}_{i\alpha}) f_{i\alpha} + \frac{1}{2}\left(\partial_t^2 + 2\partial_t \nabla \cdot \mathbf{c}_{i\alpha} + \nabla\nabla : \mathbf{c}_{i\alpha}\mathbf{c}_{i\alpha}\right) f_{i\alpha} \tag{9}$$

In order to relate LBE with a macroscopic equation, it is necessary to separate different time scales. This is to indicate different scale of physical phenomena and contribute separately in the final macroscopic equation. To do this, space and time derivative are expanded in terms of Knudsen number ε [15] as follow

[illegible] (10)

$$\nabla = \varepsilon\nabla + O(\varepsilon^2) \tag{11}$$

Expand distribution function $f_{i\alpha}$ about $f_{i\alpha}^{eq}$ gives

$$f_{i\alpha} = f_{i\alpha}^{eq} + \varepsilon f_{i\alpha}^1 + \varepsilon^2 f_{i\alpha}^2 + O(\varepsilon^3) \tag{12}$$

where

$$\sum_\alpha \sum_i f_{i\alpha}^n = \sum_\alpha \sum_i f_{i\alpha}^n \mathbf{c}_{i\alpha} = 0 \text{ for } n \geq 1 \tag{13}$$

Equation (12) imply that the non-equilibirum distribution function ($f_{i\alpha}^n$) do not contribute to the local values of density and momentum.

Substituting (10), (11) and (12) into (9) and regroup the equation to first order ε

$$(\partial_{t1} + \mathbf{c}_{i\alpha} \cdot \nabla) f_{i\alpha}^{eq} = -\frac{1}{\tau} f_{i\alpha}^1 \tag{14}$$

The equation to order ε^2 is simplified by using (14) gives

$$\partial_{t2} f_{i\alpha}^{eq} + (\partial_{t1} + \mathbf{c}_{i\alpha} \cdot \nabla)\left(1 - \frac{1}{2\tau}\right) f_{i\alpha}^1 = -\frac{1}{\tau} f_{i\alpha}^2 \tag{15}$$

A summation of (14) with respect to i and α is taken to give the first order continuity equation

$$\partial_{t1}\rho + \nabla \cdot (\rho\mathbf{u}) = 0 \tag{16}$$

Multiplying (14) by $\mathbf{c}_{i\alpha}$ and taking the summation as above

lead to

[illegible] (17)

where

$$\Pi^{eq} = \sum_{\alpha}\sum_{i}\left(\mathbf{c}_{i\alpha}\mathbf{c}_{i\alpha}\right) f_{i\alpha} \tag{18}$$

is the momentum flux tensor. After some simple mathematics manipulation to satisfy Galilean invariance and isotropic of tensor, the final expression for Π^{eq} is

$$\Pi^{eq} = c_s^2 \rho \delta_{\beta\chi} + \rho u_\beta u_\chi \tag{19}$$

Substituting (19) into (17) results in

$$\partial_{t1}(\rho \mathbf{u}) + \nabla \cdot (\rho \mathbf{u}\mathbf{u}) = -\nabla\left(c_s^2 \rho\right) \tag{20}$$

Equations (16) and (20) are the Euler equations. The pressure is given by

$$p = c_s^2 \rho \tag{21}$$

Similarly, the equation for ρ and $\mathbf{u}$ can be obtained from equations of ε^2 of (15). Taking summation with respect to i and α gives

$$\partial_{t2}\rho = 0 \tag{22}$$

Multiplying (15) by $\mathbf{c}_{i\alpha}$ and taking the summation as above gives

$$\partial_{t2}(\rho \mathbf{u}) + \nabla \cdot \left(1 - \frac{1}{2\tau}\right)\Pi^1 = 0 \tag{23}$$

where

$$\begin{aligned}\Pi^1 = -\tau\Big\{&\left(\frac{1}{3} - c_s^2\right)\partial_\gamma\left(\rho u_\gamma\right)\delta_{\beta\chi} + \frac{1}{3}\partial_\beta\left(\rho u_\chi\right) \\ &+ \frac{1}{3}\partial_\chi\left(\rho u_\beta\right) - u_\beta \partial_\chi\left(c_s^2 \rho\right) - u_\chi \partial_\beta\left(c_s^2 \rho\right) \\ &- \partial_\gamma\left(\rho u_\beta u_\chi u_\gamma\right)\Big\}\end{aligned} \tag{24}$$

Combining equations of $O(\varepsilon)$ and $O\left(\varepsilon^2\right)$ gives the correct form of the continuity equation

$$\nabla \cdot \mathbf{u} = 0 \tag{25}$$

and the momentum equation for an incompressible fluid

$$\partial_t\left(\rho u_\beta\right) + \partial_\chi\left(\rho u_\beta u_\chi\right) = -\partial_\beta\left(c_s^2 \rho\right) + \partial_\chi\left(2\rho \frac{2\tau - 1}{6} S_{\beta\chi}\right) \tag{26}$$

where $S_{\beta\chi} = \frac{1}{2}\left(\partial_\beta u_\chi + \partial_\chi u_\beta\right)$, $p = c_s^2 \rho$ and the sound speed in given by

$$c_s^2 = \frac{1}{3} \tag{27}$$

Finally, the kinematic viscosity of fluid is related to the time relaxation in mesoscopic scale as follow

$$\upsilon = \frac{2\tau - 1}{6} \tag{28}$$

From above derivations, it can be seen that the evolution equation of (7) can lead to the incompressible Navier-Stokes equation through Chapman-Enskog expansion.

III. Simulation Test case: Flow over a Blockage

The understanding of flow over a blockage is important because of its related technical problems associated with the energy conservation and the structural design bridges, towers, cars, wires, and so forth. In the building design, flow structure can significantly affect the aerodynamics characteristics such as wind load, forces and moment to the building.

Over the last twenty years, a vast amount of research activities on the flow past circular cylinder to increase the understanding of flow behavior behind the blockages. By contrast, there are very few similar studies on the other shapes although they play a dominant role in many practical applications.

Generally, the flow structures over any shape of cylinder in a 2D channel are described by two non-dimensional parameters which are Reynolds number and the blockage ratio, the ratio between the height of the blockage to that of channel height. At $Re > 1$, the flow reaches steady state exhibiting separation at the trailing edges and a symmetric motion about the horizontal centerline behind the cylinder. The length of recirculation region increases with increase in Reynolds number. The effect of instabilities which cause vortex shedding and unsteady flow can be observed when a critical Reynolds number, Re_c, is exceeded. One of objectives of this work is to determine the value of Re_c for every test case at fixed blockage ratio of 1/8.

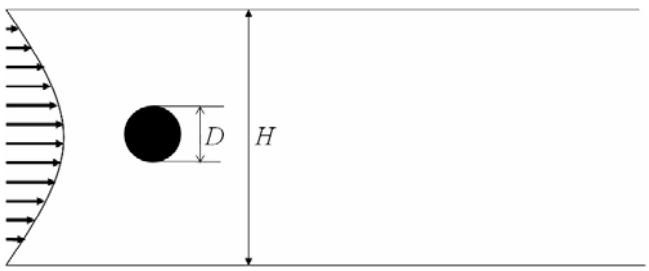

(a)

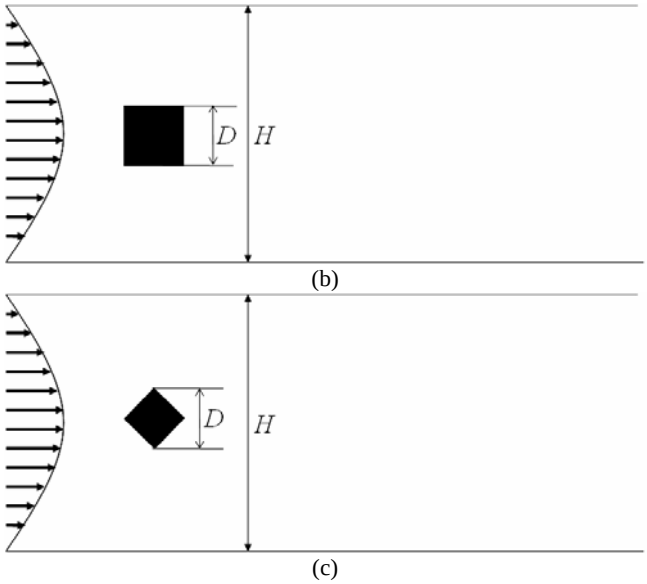

Fig. 2 Sketch of computational domain for three types of blockage inside channel flow, (a) cylinder, (b) square, and (c) diamond.

Fig. 2 shows a sketch of the geometry of the flow problem used in the present study. The blockage ratio is defined by *D/H* where *D* is the height of the cylinder and *H* is the channel height of the inflow channel. The number of lattice nodes on the height of cylinder varies between 30 and 70 depending on the value of Reynolds number.

A. Streamlines Plot

The flow with *Re* = 1 was first simulated for every case. The streamlines plots are shown in Fig. 3. It is well known that for Re ≤ 1, the creeping steady flow passes the blockage with no separation takes place [16][17].

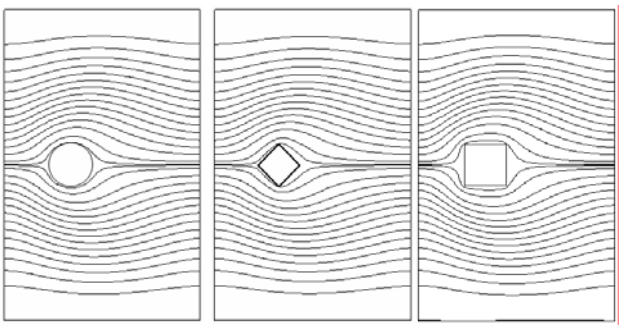

Fig. 3 Streamline plots at $\mathrm{Re} = 1$ for every tested case

As *Re* increases, the separation of flow can be firstly observed at *Re* ≈ 5 for every tested cases [18]. The flow downstream separates and formed a symmetric recirculation region. The streamline plot for *Re* = 10 is brought as reference and shown in Fig. 4.

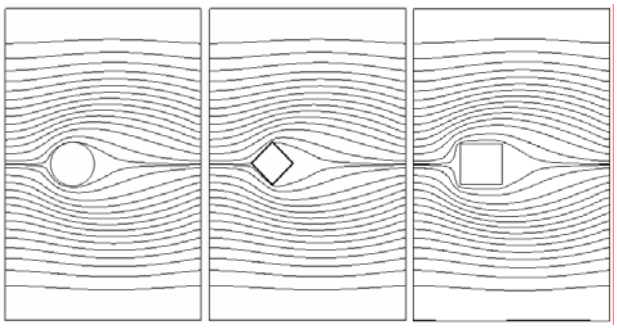

Fig. 4 Streamline plots at $\mathrm{Re} = 10$ for every tested case

B. Critical Reynolds Number

The instabilities appear causes vortex shedding and the flow becomes unsteady when critical Reynolds number, Re_c, is achieved. Re_c for flow around cylindrical blockage is found to be at 55 while for square and diamond shaped blockage are 53 and 44 respectively which are good agreement with previous studies [19][20]. Fig. 5a – 5c show the streamline plots at Re_c and a value before Re_c for every tested case. Due to the sharp separation point for diamond blockage and this lead to lowest value of Re_c for this case.

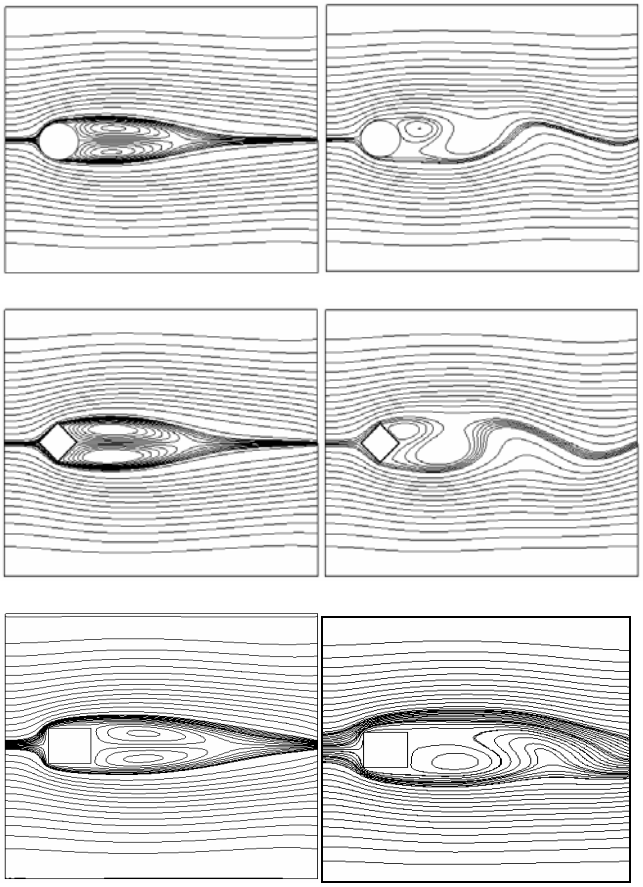

Fig. 5 Streamline plots at $\mathrm{Re}_c - 1$ and Re_c for every tested case.

C. Recirculation Length

As discussed in proceeding section, the vortices downstream the blockage are steady and symmetrical until the flow reaches critical Reynolds number. In this section, we measured the recirculation length, l_r, from the tip of cylinder in x-direction for every tested case and plotted in dimensionless form l_r/D against Reynolds numbers. The results are shown in Fig. 6. Calculated polynomial lines are also included to see the evolution of vortices. The graphs clearly show that the recirculation length increases with Reynolds numbers. The graph shows that the recirculation length downstream the square blockage developed faster that other cases due to the fix separation point at the edge of the square. In addition, unlike cylindrical and diamond blockages, when the flow begins to separate, there is no solid boundary in x-direction to decelerate the flow for the square case. However, when the flow is dominated by inertia force at high Reynolds numbers, the recirculation region length is almost the same for diamond and square blockage.

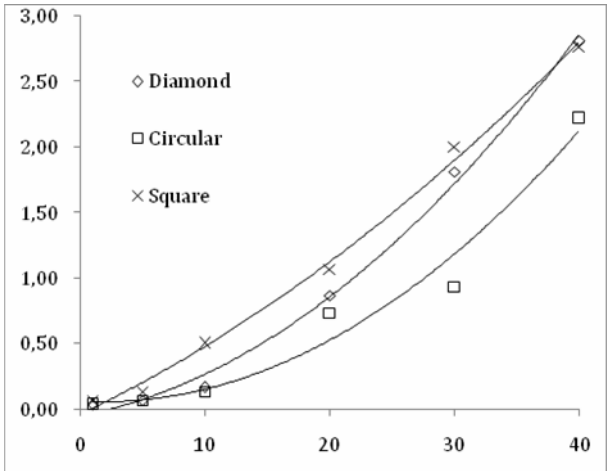

Fig. 6 Recirculation length against Reynolds number for every tested case

IV. Conclusion

Numerical predictions using lattice Boltzmann method of flow behavior past a blockage at various Reynolds number have been reported. The motivation of this study is due to the scattering of results for the flow characteristic especially the dependence of recirculation length on Reynolds number and the value of critical Reynolds number. This is evidently a lack of reliable experimental and numerical data for these flow cases. In conclusion, the present investigation with LBM has provides reliable and accurate result for 2D channel flow with blockage. This gives confidence to expand the application of LBM for the simulation at more complex fluid flow problem.

Acknowledgment

The authors would like to acknowledge Universiti Teknologi Malaysia and Malaysia government for supporting this research activity.

References

[1] X. He, and L. S. Luo, "Lattice Boltzmann model for the incompressible Navier-Stokes equation," *J. Stat. Phys.*, vol. 88, no. 3, pp. 927-944, Aug. 1997.

[2] L. Jonas, B. Chopard, S. Succi, and F. Toschi, "Numerical analysis of the averaged flow field in a turbulent lattice Boltzmann simulation," *Phys. A*, vol. 362, no. 1, pp. 6-10, Mar. 2006.

[3] S. Chen, and G. Doolen, "Lattice Boltzmann method for fluid flows," *Ann. Rev. Fluid Mech.*, vol. 30, no. 1, pp. 329-364, Jan. 1998.

[4] I. Halliday, and C. M. Care, "Steady state hydrodynamics of lattice Boltzmann immiscible lattice gas," *Phys. Rev. E*, vol. 53, no. 2, pp. 1602-1612, Jul. 1996.

[5] G. Breyiannis, and D. Valougeorgis, "Lattice kinetic simulations in three-dimensional magnetohydrodyanmics," *Phys. Rev. E*, vol. 69, no. 6, pp. 065702/1-065702/4, Jun. 2004.

[6] C. S. N. Azwadi, and T. Tanahashi, "Three-dimensional thermal lattice Boltzmann simulationof natural convection in a cubic cavity," *Intl. J. Mod. Phys. B*, vol. 21, no. 1, pp. 87-96, Jan. 2007.

[7] X. Shan, and H. Chen, "Lattice Boltzmann model for simulating flows with multiple phases and components," *Phys. Rev. E*, vol. 47, no. 3, pp. 1815-1820, Nov. 1993.

[8] S. Hou, Q. Zou, S. Chen, G. Doolen, and A. C. Cogley, "Simulation of cavity flow by the Lattice Boltzmann method," *J. Comp. Phys.*, vol. 118, no. 2, pp. 329-347, May. 1995.

[9] P. L. Bhatnagar, E. P. Gross, and M. Krook, "A Model for collision process in gases. 1. Small amplitude processes in charged and neutral one-component system," *Phys. Rev.*, vol. 70, no. 3, pp. 511-525, Nov. 1954.

[10] D. A. Gladrow, *Lattice Gas Cellular Automata and Lattice Boltzmann Models*. New York: Springer-Verlag, 2000, ch. 5.

[11] Y. H. Qian, D. Humieres, and P. Lallemand, "Lattice BGK for Navier-Stokes equation," *Europhys. Lett.*, vol. 17, no. 6, pp. 479-484, Feb. 1992.

[12] X. Shan, X. Feng, and H. Chen, "Kinetic theory representation of hydrodynamics: a way beyond the Navier-Stokes equation," J. F. Mech., vol. 550, pp. 413-441, Mar. 2006.

[13] C. S. N. Azwadi, and T. Tanahashi, "Simplified thermal lattice Boltzmann in incompressible limit," *Intl. J. Mod. Phys. B*, vol. 20, no. 17, pp. 2437-2449, Jul. 2006.

[14] G. McNamara, and B. Alder, "Analysis of the lattice Boltzmann treatment of hydrodynamics," *Phys. A*, vol. 194, no. 1, pp. 218-228, Mar. 1993.

[15] C. Cercignani, *Theory and Application of Boltzmann Equation*. Elsevier Science, 1975, ch. 3.

[16] R. W. Davis, E. F. Moore, and L. P. Purtell, "A numerical-experimental study of confined flow around rectangular cylinders," *Phys. Fluids*, vol. 27, no. 1, pp. 46-59, Jan. 1984.

[17] J. Bernsdorf, M. Breuer, T. Zeiser, and F. Durst, "Accurate computations of the laminar flow past a square cylinder based on two different methods: Lattice Boltzmann and finite volue," *Intl. J. Heat and Fluid Flow*, vol. 21, no. 2, pp. 186-196, Apr. 2000.

[18] A. Okajima, "Strouhal numbers of rectangular cylinders," *J. Fluid. Mech.*, vol. 123, pp. 379-398, Apr. 2006.

[19] K. M. Kelkar, and S. V. Patankar, "Numerical prediction of vortex shedding behind a square cylinder," *Intl. J. Numer. Meth. Fluid*, vol. 14, no. 3, pp. 327-341, Feb. 1992.

[20] H. Suzuki, Y. Inoue, T. Fukutani, and K. Suzuki, "Unsteady flow in a channel obstructed by a square rod (crisscross motion of vortex)," *Intl. J. Heat Fluid Flow*, vol. 14, no. 1, pp. 2-9, Mar. 1993.